Research article

Corrosion inhibition study of 6061 aluminium alloy in the presence of ethyl 5-methyl-1-(4-nitrophenyl)-1H-1,2,3-triazole-4-carboxylate (NTE) in hydrochloric acid☆

K. Raviprabha [a], Ramesh S. Bhat [b,*], Subrahmanya I. Bhat [b], P. Nagaraj [c], K. Jyothi [d]

[b] NITTE (Deemed to be University), Department of Chemistry, NMAM Institute of Technology (NMAMIT), Nitte, 574110, India
[a] Department of Chemistry, Shri Madhwa Vadiraja Institute of Technology & Management, Bantakal, Udupi, 574115, Karnataka, India
[c] Department of Chemistry, Yenepoya Institute of Technology, Karnataka, India
[d] Department of Chemistry, St. Joseph Engineering College, Mangalore, 575028, India

ARTICLE INFO

ABSTRACT

The inhibitory effect of an ethyl 5-methyl-1-(4-nitrophenyl)-1H-1,2,3-triazole-4-carboxylate (NTE) was investigated on the corrosion of Al (AA6061) alloy at different temperatures (303–333 K) by Electrochemical impedance spectroscopy (EIS), Potentiodynamic polarization (PDP), and weight loss techniques. It was found that NTE molecules protect the aluminium against corrosion and its ability increases with increasing concentrations, and temperature resulting in better inhibitory performance. At all concentrations and temperature ranges, NTE exhibited mixed inhibitor action and complied with the Langmuir isotherm. At 100 ppm and 333 K, NTE demonstrated the highest inhibition efficiency (94%). The EIS results and the PDP results had a good level of concordance. A suitable mechanism for the corrosion prevention of AA6061 alloy was proposed. Atomic force microscopy (AFM) and scanning electron microscopy (SEM) were used to confirm the adsorption of an inhibitor onto the aluminium alloy surface. The electrochemical results were validated by morphological examination, which demonstrated that NTE prevents uniform corrosion of aluminium alloy in acid chloride solutions. The activation energy and thermodynamic parameters were computed, and the results were discussed.

1. Introduction

Aluminium and its alloys are commonly employed in the marine, automobile, and aircraft sectors because of their excellent corrosion resistance, appropriate extrusion, and rolling properties [1]. Acidic solutions are needed in many industrial applications, including industrial cleaning, pickling, and other industrial preparative procedures. Corrosion inhibitors (CI) are widely employed to lessen the corrosive attack on items containing metals as a result of the aggressiveness of acidic media [2,3]. The CIs should be selected based on the properties of the system, the kind of acidic medium, the temperature of the solution, the concentration, the presence of dissolved inorganic or organic components, and in particular, the type of metallic elements. The CIs come in a wide variety of forms and compositions. For instance, organic substances operate as adsorption-type inhibitors by adhering to metal surfaces to halt metal
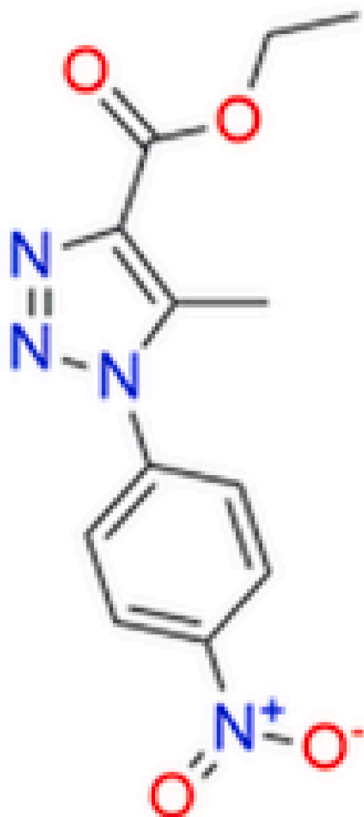

Fig. 1. Ethyl 5- methyl-1-(4-nitrophenyl)-1,2,3-triazole-4-carboxylate (NTE).

dissolution and reduction reactions [4]. The organic CIs have better film-forming capabilities, may be utilized at low concentrations, and are less hazardous than the inorganic ones [5]. The presence of both-electrons from aromatic rings and heteroatoms in the molecular structures is mainly responsible for the adsorption characteristics of organic CIs [6]. In fact, a lot of research has been done on organic compounds containing nitrogen, phosphorus, sulphur, and oxygen atoms as CIs for metals and their alloys in acidic conditions [7]. The Al–Mg and Al–Mg–Si alloys are the commonly used aluminium alloys for use in corrosive environments. Al alloys have demonstrated high corrosion resistant qualities because when in contact with a neutral solution or environment, they can produce a stable Al_2O_3 barrier on the surface [8]. When the metal is subjected to strong concentrations of acids or bases, this amphoteric surface coating dissolves [9]. Therefore, in these circumstances, excessive metal dissolution should be prevented by the addition of an appropriate inhibitor to the solution. Even if there are numerous ways to counteract corrosion, the simplest and most practical approach is to add a suitable inhibitor to the corrosive media [10].

Triazole, which is five members and three nitrogen atoms, serves as the foundation for numerous compounds with a wide range of uses, particularly in medicine [11]. Due to their outstanding qualities, these triazole derivative compounds have garnered the attention of numerous researchers. They possess a range of biological, industrial, and agricultural properties, as well as antibacterial, antitubercular, anti-inflammatory, and diuretic actions [12]. Recently, a lot of study has concentrated on using environmentally friendly corrosion inhibitors. Due to their low toxicity and high chemical activity, these substances can be regarded as ecological inhibitors [13]. These triazole derivatives are especially attracted to metal surfaces with water molecules moving on the surface. They are naturally amphoteric and combine with acids and bases to generate salts. Moreover, they have a lot of p-electron abundance and unshared electron pairs on the nitrogen atom, which when combined with the d-orbitals of the metal, can provide a protective coating [14]. As a result, 1,2,4-triazole derivative use as corrosion inhibitors was the focus of several previous research papers [15]. For instance, El Hajjaji et al. [16] shown that when utilized at a concentration of 1.0×10^{-3} M in 2 M H_3PO_4 [17], 3,5-bis (disubstituted)-4-amino-1,2,4-triazole derivatives have a corrosion prevention efficacy of 86% for mild steel. Recent studies have looked at 5-hexyl sulfanyl-1,2,4-triazole (HST) and 1-*p*-tolyl-1H-1,2,3-triazol-4-yl methanol (TTM) as synthetic heterocyclic compounds to inhibit the corrosion of steel in 1 M HCl [18,19]. These inhibitors achieved a good inhibition efficiency of 97% and 81%, in 1 M HCl respectively.

The organic molecules with heteroatoms, electron-donating functional groups, and linkages are the most potent inhibitors [20–22]. It has been observed that various organic compounds with polar functionalities including N, O, and S atoms and aromatic hydrocarbons in a conjugated system are efficient inhibitors of corrosion for aluminium alloys [23,24]. A thorough analysis of the corrosion of AA6061 is required, followed by the creation of an effective corrosion inhibitor for AA6061 that is simple to use and has outstanding

inhibitory efficacy. Because of the interaction of the π-orbital with the metal surface, compounds with π-bonds usually have good inhibition properties. Due to the presence of these structural characteristics, several Schiff bases have previously been described as corrosion inhibitors for aluminium alloys [25]. In the current work at various temperatures, we aim to exploit the corrosion inhibition activity of NTE to the surface of Al alloy in the presence of 0.1 M HCl.

2. Experimental procedures

2.1. Material

The material used in the experiment was Al alloy. The weight % of elements present in this alloy consists of Mg (0.84), Si (0.49), Mn (0.17), Fe (0.66), Cu (0.18), Cr (0.06), and Al (balance).

2.2. Preparation of specimen sample

For the weight loss procedure, Al (AA6061) alloy specimens of 2 cm × 2 cm × 1 cm were used. Al alloy specimens were polished with various grades of emery papers (100, 300, 400, 500, 800, and 1200) to remove the oxide film and other impurities and then cleaned using distilled water, and dried with acetone. For electrochemical investigations, the cylindrical Al rod with 1.31 cm^2 exposed area was designed and the lingering portion was encased in epoxy gum. Using emery papers and then levigated alumina, the cylindrical rod was polished. Acetone was used to dry the Al alloy specimen after it had been washed with distilled water.

2.3. Preparation of corrosive media

0.1 M HCl was made with deionized water and 37% analytical-grade (Merck) reagent of hydrochloric acid. The volumetric method was used to standardize HCl using a normal NaOH solution. As and when needed, HCl solution at the desired concentration (0.1 M) was produced from the standard solution. At 303, 313, and 323 K, experiments with unstirred and aerated conditions were conducted using a calibrated thermostat. The 20–100 ppm of NTE in HCl solutions were used to study the inhibitory effect. Fig. 1 shows the chemical structure of Ethyl 5- methyl-1-(4-nitrophenyl)-1,2,3-triazole-4-carboxylate.

2.4. Weight-loss technique

The Al alloy specimens of size 2 cm × 2 cm × 1 cm were used for weight loss measurements. The specimens were dipped in 200 ml of 0.1 M HCl solution and taken in a 100 ml beaker having different concentrations of the NTE for around 5 h at 303 K. The coupons were then taken out of the test liquids and wiped with absorbent cotton before being cleaned, left to dry, and weighed [25]. Three times each measurement was made, and the mean result was used for the estimation.

2.5. Electrochemical method

Al alloy was subjected to electrochemical studies using an electrochemical workstation (CH604 E, and CH-instrument) with a three-electrode glass cell, the working electrode is an Al alloy specimen of size 1.31 cm^2, the reference electrode is a saturated calomel, and the counter electrode is platinum, polarization experiments and electrochemical impedance measurements (EIS) was conducted. The freshly polished specimen was given time to set up a stable state open circuit potential (OCP) at various temperatures by subjecting it to 0.1 M HCl with or without NTE. PDP curves were produced for the OCP by polarizing the specimen from - 250 mV cathodically to +250 mV anodically at a scanning frequency of 0.01 mV/s. A calibrated thermostat was used to run the trials at various temperatures. To measure the corrosion potential (CP) and corrosion current densities (c.c.d), to determine the corrosion rate (CR) and the percentage efficiency of the inhibitor. To carry out the EIS investigations, a 10 mV, AC signal with a frequency range of 100000 Hz–0.01 Hz was impressed onto the OCP. Impedance readings were analyzed using Nyquist curves to assess corrosion properties [25]. Based on the equivalent circuit fitting produced by modeling the impedance data with the ZSimpWin version 3.21 software, the double layer capacitance (DLC) and the charge transfer resistance were determined.

2.6. Surface characterization

At a 1000× magnification, analytical scanning electron microscopy (JEOL JSM-6380L) was employed to analyze the surface structure of Al. The metal samples were soaked in an HCl medium for 10 h, both with and without the inhibitor, to determine the surface morphology. The roughness of the Al alloy specimen with and without NTE was checked using AFM (IB342-Innova model).

3. Results and discussion

3.1. Weight loss method

The weight loss (WL) of Al alloy (AA6061) in 0.1 M HCl was investigated both with and without NTE concentration. The inhibition efficiency is calculated using equation (1).

Table 1

Weight-loss for Al alloy, corrosion inhibition in different concentrations of NTE at various temperatures.

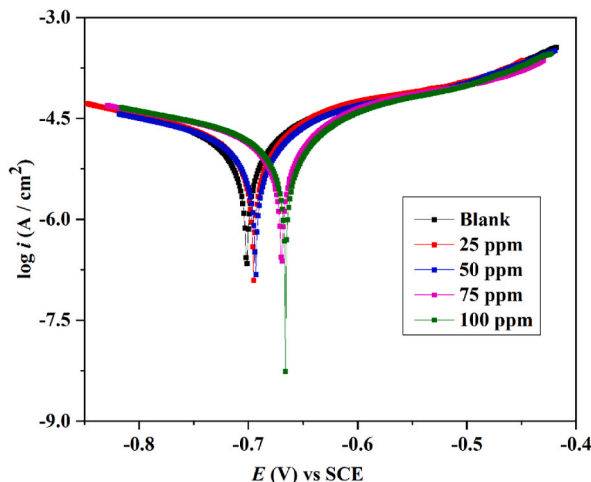| Conc. (M)	Conc. (ppm)	303K		313K		323K		333K	
		CR (mm y^{-1})	I.E. (%)	CR (mm y^{-1})	I.E. (%)	CR (mm y^{-1})	I.E. (%)	CR (mm y^{-1})	I.E. (%)
0.1	Blank	2.250	–	2.800	–	3.241	–	3.701	–
	25	0.418	81.40	0.425	84.80	0.451	86.10	0.511	86.20
	50	0.385	82.90	0.400	85.70	0.364	88.80	0.403	89.10
	75	0.355	84.20	0.375	86.60	0.296	90.90	0.325	91.20
	100	0.306	86.40	0.325	88.40	0.263	91.90	0.289	92.20

Fig. 2. PDP curves for the corrosion of Al alloy containing variable NTE concentrations in 0.1 M HCl at 303K.

$$IE(\%) = \frac{W_{un} - W_{in}}{W_{un}} \times 100 \tag{1}$$

in this equation, W_{un} and W_{in} indicate the WL of the Al alloy dipped in 0.1 M HCl without and with NTE, at 303 K. The CR is calculated by using equation (2).

$$CR(\text{mm / year}) = 87.6 \times (W / \rho A t) \tag{2}$$

in this equation, W signifies the weight loss (g dm^{-3}), ρ denotes the density (2.7 g cm^{-3}), A is the area (cm^2) of the sample, and t implies the immersion time (h). The CR and I.E., are presented in Table 1, which indicates that the CR decreases with an increase in the concentration of NTE in the acid medium. As a result, the I.E., increased with increasing NTE concentration, and it reached a maximum value of 92.2% at 100 ppm.

3.2. Electrochemical analysis

3.2.1. Polarization (PDP) analysis

Using potentiodynamic polarization at 303 K, the degradation of an Al alloy in 0.1 M HCl in the presence and absence of the inhibitor (NTE) was examined. The PDP plot is shown in Fig. 2. Similar plots were obtained at various temperatures in 0.1 M hydrochloric acid at different concentrations of NTE. The corrosion potential (E_{corr}), (βc) and anodic (βa) Tafel slopes, and corrosion current density (i_{corr}) of polarization were obtained using PDP plots. i_{corr} was then used to compute the corrosion rate (CR), efficiency of inhibition (I.E.) using equations (3) and (4) respectively.

$$CR = \frac{3270 \times M \times i_{corr}}{\rho \times z} \tag{3}$$

where ρ is the density of the material that is corroding (2.7 g/cm^{-3}), the atomic mass (M), and the number of electrons (Z) transferred per metal atom [26]. The %. I.E is given by equation (4).

$$\eta = \frac{i_{corr(un)} - i_{corr(in)}}{i_{corr(un)}} \times 100 \tag{4}$$

Table 2

PDP data for the corrosion of Al alloy containing varying concentrations of NTE.

| Temp. (K)	Conc. (ppm)	$-E_{corr}$ (V)	βa (1/V)	βc (1/V)	i_{corr} ($\mu A/cm^2$)	I.E (%)
303	Blank	0.7011	6.58	5.45	1.894	–
	25	0.6950	7.15	5.24	0.359	81.00
	50	0.6931	7.25	5.57	0.301	84.10
	75	0.6691	7.34	5.65	0.271	85.60
	100	0.6662	7.40	5.75	0.241	87.20
313	Blank	0.7185	4.26	3.61	3.352	–
	25	0.7165	4.66	3.71	0.413	87.40
	50	0.7153	4.83	3.80	0.338	89.70
	75	0.7096	4.97	3.85	0.275	91.60
	100	0.6993	5.27	3.93	0.246	92.50
323	Blank	0.7085	3.71	5.08	6.458	–
	25	0.7078	3.86	5.44	0.696	88.10
	50	0.6956	3.92	5.48	0.506	91.30
	75	0.6909	4.29	5.58	0.428	92.60
	100	0.6854	4.81	5.63	0.377	93.40
333	Blank	0.7432	4.59	5.16	12.43	–
	25	0.6801	4.76	5.20	1.301	88.50
	50	0.6768	4.89	5.46	0.843	92.50
	75	0.6688	5.25	5.55	0.694	93.80
	100	0.6524	5.68	5.66	0.648	94.20
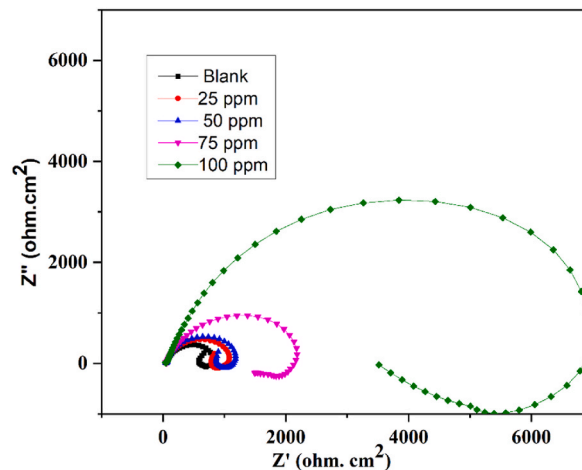
Fig. 3. EIS curves for the corrosion of Al alloy in 0.1 M HCl at 303 K with NTE concentration.

where corrosion current densities without and with the inhibitor are i_{corr} *(un)* and i_{corr}*(in)*, respectively. Table 2 shows the outcomes of PDP tests for the corrosion of Al alloy in 0.1 M HCl at different temperatures and different concentrations of inhibitor. When different inhibitor concentrations are present, the corrosion current density, and CRs are decreased. As a result, as the inhibitor concentration increases, so does the inhibition efficiency. The I.E, was highest at 333K (94.2%). This is the main cause of the adsorption of inhibitor on the Al surface. The adsorbed inhibitor provides a shielding between the Al surface and the hostile liquid [27]. If the CP of the inhibitor solution is less than 85 mV when compared to the uninhibited solution, the inhibitor can be categorized as anodic or cathodic, according to the literature [28–30]. However, the maximum displacement in the present study was considerably 85 mV. This implies that NTE might function as a mixed-type of inhibitor, with anodic inhibition dominating. As a result, it is possible that NTE functions as a mixed-type inhibitor with a preference for anodic inhibition. Indicating that the evolution of hydrogen is activated-controlled and has no impact on the mechanism of the reduction process, the morphologies of the PDP curves with and without inhibitor (Fig. 2) are similar [31]. The slopes of both the cathodic (βc) and anodic (βa) Tafel lines did not vary significantly when the inhibitor concentration is raised. The additional inhibitor hinders the anodic oxidation by halting the anodic reaction as well as helping to passivate an oxide coating on the metal surface. This indicates how the NTE which is under investigation works as a mixed-type inhibitor. The results in all tables demonstrate a drop of the i_{corr} value after the inhibitor has been added. Data demonstrates that, as the inhibitor concentration rises, the efficiency of inhibition increases. The explanation for this is the adsorption inhibitors on the AA6061 layer. The literature suggests that [32,33] if E_{corr} was lower than +85 mV or −85 mV as compared to the unrestrained liquid, the inhibitor is categorized as anodic or cathodic. In this study, the biggest shift was lower than +85 mV or −85mV. In this case, anodic inhibition takes precedence over NTE's mixed inhibitory effects. A comparison of polarization curves shows that gas generation is controlled while reduction
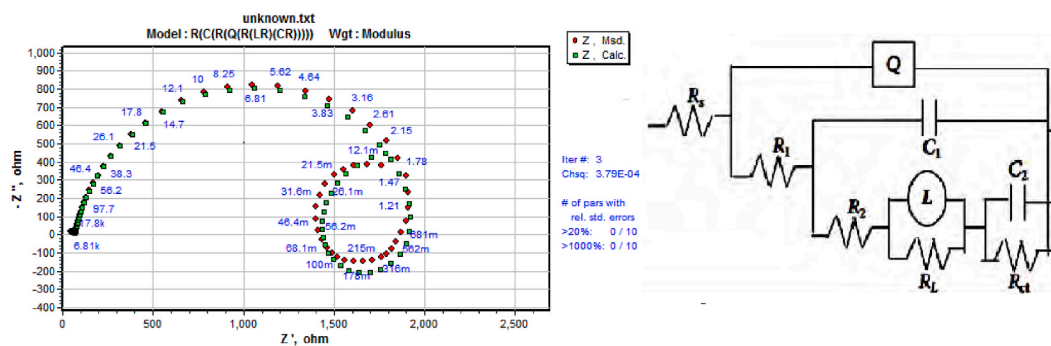
Fig. 4. Equivalent circuit fitment for the experimental EIS data.

Table 3
EIS data for the corrosion AA6061 in 0.1 M HCl containing variable NTE concentrations.

Temp (K)	Conc (ppm)	Rp (Ωcm^2)	C_{dl} (μF)	I.E (%)
303	Blank	20.50	2085.00	–
	25	81.63	134.00	74.89
	50	103.35	100.00	80.16
	75	110.21	59.16	81.40
	100	152.00	50.48	86.51
313	Blank	12.30	5761.00	–
	25	68.18	309.43	81.96
	50	85.00	285.06	85.53
	75	99.90	202.18	87.69
	100	123.50	133.02	90.04
323	Blank	7.50	12936	–
	25	63.70	683.81	88.23
	50	69.30	616.76	89.18
	75	88.19	398.42	91.50
	100	106.47	320.33	92.96
333	Blank	4.20	55870	–
	25	50.50	2642.90	91.68
	50	58.90	1166.10	92.87
	75	68.25	993.51	93.85
	100	74.40	736.57	94.35

reaction mechanisms are unaffected [34,35]. With increasing inhibitor concentration, Tafel lines did not distinguish appreciably, demonstrating that gas production is regulated by activation and that the addition of a blocker has no effect on the inhibitory mechanism. The additional inhibitor inhibits anodic oxidation and aids passivation of the oxide deposit on the metal surface, as well as stopping the anodic reaction.

3.2.2. EIS studies

EIS experiments were carried out to determine overall protection against corrosion of metal surfaces, over time. From EIS studies, Nyquist plots were obtained. EIS studies were performed on AA6061 for uninhibited and inhibited HCl medium containing different concentrations of NTE.

At 303 K, Fig. 3 shows Z′ vs. Z″ plots in 0.1 M HCl solution with different NTE concentrations. The radius of the semicircle in Nyquist plots due to irregular surfaces, and porous layer growth [36]. The frequency distribution of interfacial impedance is caused by the coarseness and non-regularity of the surface of the electrode, the adsorption of the inhibitor, and the development of porous layers, which causes the Nyquist plots to diverge semicircle shapes [37]. A semicircle was visible in the impedance spectrum, which shows that the charge transfer process mostly controls corrosion. Fig. 3 illustrates a large capacitive loop in the high-frequency area and a small inductive loop in the low-frequency area. The growth of a layer on the metallic surface and charge transfer during the corrosion process is represented by the big capacitive loop [38]. Low-frequency loop corresponds to the relaxation process of adsorption by H^+ and Cl^- ions onto the oxide film [39]. Chloride ions, oxide ions, or other charged species may bind to the electrode surface and be incorporated there. It may be connected to the loop [20]. From the Nyquist plot, the width of the capacitive loop increased with an increase in the concentration of the inhibitor. It is caused by a reduction in CR due to the adsorption of the inhibitor onto the metal surface. The equivalent circuit that was utilized to simulate the impedance curve for Al alloy is shown in Fig. 4. There are nine components in the equivalent circuit. They are the inductive resistance (R_L), inductive element (L), solution resistance (Rs) as well as charge transfer resistance (Rct). The C_1 and C_2 are the capacitors in series, and the R_1, R_2, R_L, and Rct are the series of resistors parallel to the constant phase element (CPE) Q. The inductors L and R_L are in parallel. A resistor parallel circuit is ascribed to an oxide film
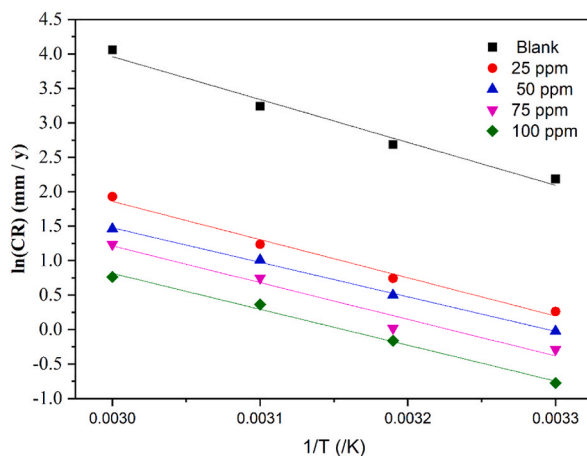
Fig. 5. Plot of ln (CR) vs. 1/T for the corrosion of Al alloy with variable NTE concentrations in 0.1 M HCl.

because of ionic conduction of the oxide layer, and capacitance because of its dielectric characteristics. Equations (5) and (6) can be used to calculate the polarization resistance (Rp) and double-layer capacitance, respectively:

$$R_p = R_1 + R_2 + R_L + R_{ct}$$ (5)

$$C_{dl} = C_1 + C_2$$ (6)

The EIS data were given in Table 3. The CPE was determined using equation (7).

$$Z = A^{-1}(iw)^{-n}$$ (7)

where w is angular frequency, i is imaginary number, A is proportionality constant, n is the exponent relating to the phase shift. The CPE behaves exactly like a perfect capacitor if n = 1. Equation (8) was used to compute the capacitance correlation to its real value.

$$C_{dl} = \frac{1}{2\pi f_{max\ Rct}}$$ (8)

The charge transfer resistance (R_{ct}), and f_{max} is the frequency at which the imaginary component of impedance is maximum. Table 3 shows that the measured C_{dl} value at all temperatures decreased with increasing inhibitor concentrations due to a raise in the electrical double layer at the metal -solution interface. The steady substitution of inhibitor molecules for water molecules led to a further drop in C_{dl} values. The i_{corr} was inversely correlated with the R_P. Using Equation (9), the inhibition efficiency was calculated.

$$I.E\ (\%) = \frac{Rp\ inh - Rp}{Rp(inh)} \times 100$$ (9)

where Rp and Rp (inh) are, respectively, the polarization resistances in the presence or absence of the inhibitor. The concentration of the inhibitor increases along with the R_P values. The fact that the value of double layer capacitance (C_{dl}) decreases as a result shows that the charge transfer process primarily regulates the corrosion reactions. Nine elements form the equivalent circuit. The growth of an electrical double layer at the metal-solution interface is caused by the decrease in the Cdl value. C_{dl} values continue to fall as inhibitor molecules are slowly replaced by water molecules. The values of polarization resistance (R_P) are inversely proportional to the corrosion current density (i_{corr}). C_{dl} falls, R_P rises, and inhibition values rise when inhibitor concentration rises.

3.2.3. Impact of temperature on the performance of NTE inhibition

The fluctuation of the CR with temperature in the presence and absence of inhibitors was visually examined to determine kinetic parameters. The action of adsorption was seen by fitting the results into appropriate adsorption isotherms, and thermodynamic parameters were calculated using the same way.

3.3. Kinetic parameter evaluation

The thermal impact of corrosion inhibition of AA6061 is investigated with NTE at temperatures of 303–333 K. Rate of corrosion and NTE efficiency both have been demonstrated to increase, as the medium temperature rises. The enhanced corrosion rate is attributable to the increased conductivity of the electrolyte as well as the increased rate of aggressive ion transfer at higher temperatures. PDP and EIS studies however retained the shape of the plot. This finding suggests that temperature affects corrosion rates without modifying the mechanism of corrosion. The energy of activation (Ea) was calculated from Arrhenius equation (Equation (10)). Fig. 5 ln (CR) vs. 1/T plots for Al alloy in various concentrations of NTE in 0.1 M hydrochloric acid. The plot of ln (CR) vs. 1/T gave a straight line with an

Table 4
Temperature-dependent activation parameters for the Al alloy in 0.1 M HCl with different NTE concentrations.

HCl	Conc. (ppm)	Ea (kJ/mol)	ΔH (kJ/mol)	-ΔS (J/mol/K)
0.1 M	Blank	52.76	50.11	186.10
	25	39.16	33.95	127.50
	50	31.59	26.61	153.60
	75	30.81	25.61	158.38
	100	29.86	24.66	160.54
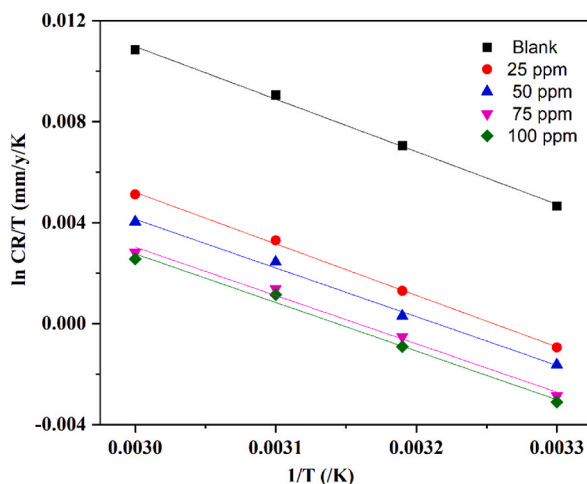
Fig. 6. Plot of ln CR/T vs. 1/T with variable NTE concentrations in 0.1 M HCl.

average correlation coefficient of $R^2 = 0.998$ and a slope of Ea/R, the activation energy for both corrosion and corrosion inhibition were calculated.

$$\ln(CR) = A - \frac{Ea}{RT} \tag{10}$$

where absolute temperature T, the universal gas constant R, the energy of activation Ea, and the Arrhenius constant A. The enthalpy $[\Delta H^{\neq}]$ and entropy of activation $[\Delta S^{\neq}]$ for dissolution of metal was calculated using equation (11).

$$CR = \frac{RT}{Nh} \exp\left(\frac{\Delta S^{\neq}}{R}\right) \exp\left(\frac{-\Delta H^{\neq}}{RT}\right) \tag{11}$$

The intercept $= \ln RT/Nh \exp [(S)/R]$ provided the value of entropy of activation, which is reported in Table 4. The plot of ln CR/T vs. 1/T at different concentrations as shown in Fig. 6, and gave a collinear line $[R^2 = 0.999]$ with slope matching to $[\Delta H^{\neq}/R]$ which gave the value of enthalpy of activation and from the intercept $= \ln \frac{RT}{Nh} \exp\left[\frac{\Delta S^{\neq}}{R}\right]$ entropy of activation is obtained. The activation energy (Ea) reduced as the concentration of the inhibitor increased because of the progressive adsorption of inhibitor molecules to Al alloys, even while the reduction in Ea of the inhibited solution favors chemical adsorption of the inhibitor on metal surfaces. Chemisorption is the process of transferring charges from the NTE molecule to the Al surface to develop a coordinate bond. The large negative values of entropy of activation (EA) imply a decrease in the randomization from the reactants to the triggered complex, suggesting that the activated complex is an association rather than a dissociation [40,41]. The slow rate of adsorption of inhibitor was observed during at higher temperatures, resulting in a closer approach to equilibrium [42]. The transfer of the net corrosion reaction from the uncovered to the covered section of the metal surface causes a decrease in corrosion activation energy at increasing levels of inhibition [43].

3.4. Thermodynamic parameter evaluation-isotherm of adsorption

The adsorption isotherm, also known as the Langmuir, Temkin, Frumkin, and Flory–Huggin's isotherm, shows clear adsorption mechanism. The isotherms were fitted with the surface coverage degrees that were discovered by PDP. The Langmuir adsorption isotherm for monolayer chemisorption provides the greatest fit when the slopes and linear regression coefficient (R^2) are close to 1. The C_{inh}/Θ vs. C_{inh} is plotted in Fig. 7 as a straight line with a 1/k intercept. Equation (12) gives Langmuir adsorption isotherm:
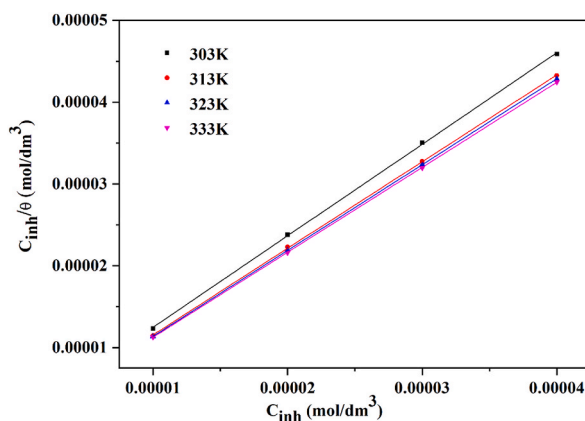
$$\frac{Cinh}{\theta} = \frac{1}{K} + Cinh \tag{12}$$

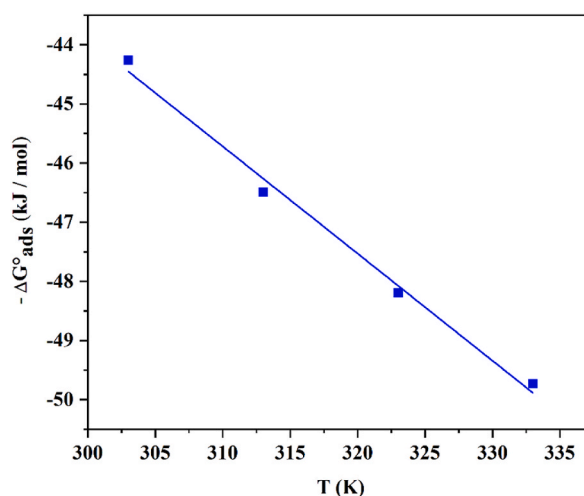**Fig. 7.** Langmuir isotherms for NTE in 0.1 M HCl for Al alloy.

Fig. 8. Plot of ΔG°_{ads} vs. T for the adsorption of NTE in 0.1 M HCl on the Al alloy.

Table 5
Temperature dependent thermodynamic variables for the adsorption of NTE on the surface of AA6061 in Hydrochloric acid.

HCl(M)	Temp.	Slope	R^2	ΔG°_{ads} (kJ/mol)	ΔS°_{ads} (kJ/mol/K)	ΔH°_{ads} (kJ/mol)
0.1	303K	1.11843	0.99977	−44.26	−0.1811	10.42
	313K	1.05859	0.99989	−46.49		
	323K	1.04919	0.9999	−48.19		
	333K	1.03852	0.99998	−49.73		

Where C_{inh} is the inhibitor concentration, K equilibrium constant for the inhibitor – metal interaction, and θ is surface coverage. Equation (13) was used to determine the standard change in free energy (ΔG°ads) for the adsorption.

$$K = \frac{1}{55.5} \exp\left(\frac{\Delta G^{\circ} \, ads}{RT}\right) \tag{13}$$

Fig. 8 show the plot of ΔG^0_{ads} against T. Intercept and slope of the straight line were used to determine the standard enthalpy of adsorption (ΔH^0_{ads}) and standard entropy of adsorption (ΔS^0_{ads}) which are shown in Table 5. Negative ΔG^0_{ads} levels ensured the impulsiveness of the adsorption process. The normal ΔG^0_{ads} values reported in the literature [44,45] are around 20 kJ mol^{-1} or less. Physisorption is implied by the ΔG^0_{ads} value up to −20 kJ mol^{-1}, while chemisorption is implied by values larger than −40 kJ mol^{-1}, according to the literature [46]. The values of the ΔG°ads for the adsorption of NTE on the AA6061 surface in the studied concentrations of hydrochloric acid is more than −40 kJ mol^{-1} indicated that the adsorption of NTE on the surface of AA6061 may involve chemisorption processes. According to the reported literature [47,48] if the enthalpy of adsorption (ΔH°ads) is positive then the adsorption
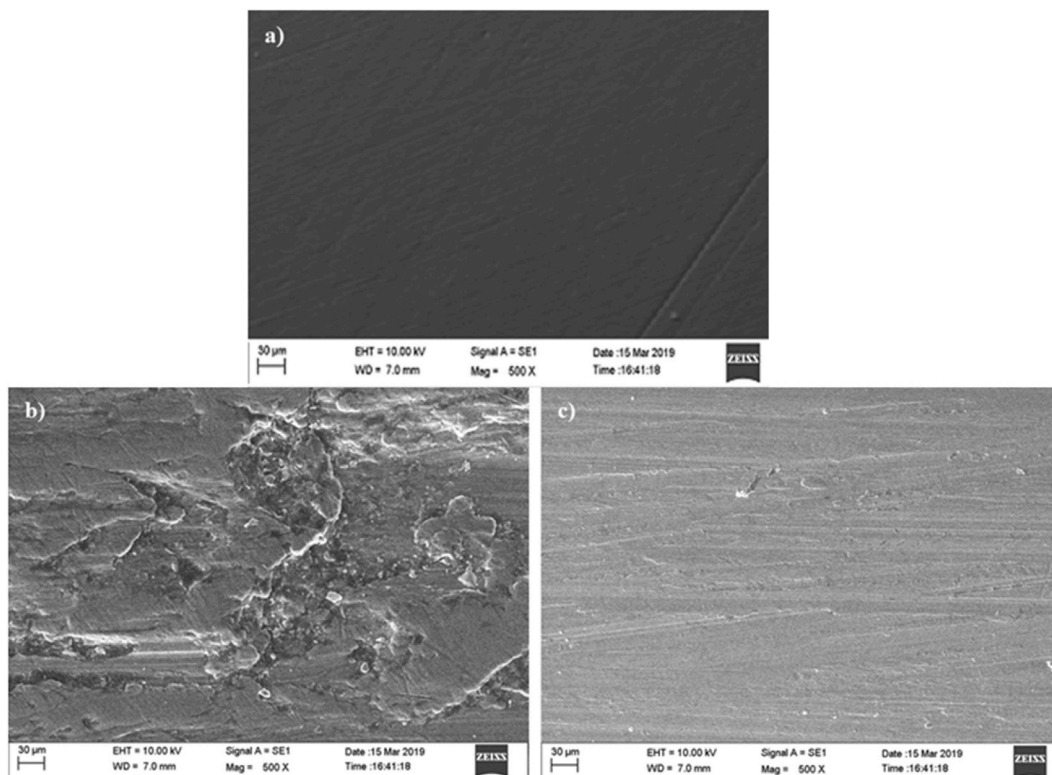
Fig. 9. SEM images of Al alloy dipped in 0.1 M HCl for 24 h at 298 K: (a) polished Al, (b) before inhibition, and c) after inhibition.

of the inhibitor onto the metal surface takes place by chemisorption. In this case the value is 10.42 kJ mol^{-1}. The entropy of adsorption (ΔS°_{ads}.) value is negative, indicating that an ordering took place when the inhibitor gets adsorbed on the metal surface.

3.5. Surface morphology studies

Fig. 9 shows the SEM images of Al alloy before and after dipping in 0.1 M HCl with, and without NTE. SEM image shows an increase in the smoothness of the surface of Al alloy after the addition of inhibitor (NTE). The SEM topography of polished of Al alloy surface is shown in Fig. 9a. It reveals that polished specimen shows a uniform, crack free surface. Fig. 9b, however, demonstrates deep trenches that were created because of the strong acid medium attack. A smooth surface with few holes was visible in the SEM image of the inhibited Al alloy surface is shown in Fig. 9c. This shows that the adsorption of NTE has significantly reduced the aggressive action of 0.1 M HCl.

Atomic force microscopy (AFM) was used to analyze the surface of an Al alloy immersed in 0.1 M HCl for 24 h at 298 K with and without inhibitors. The SEM micro-images only offer qualitative details about the surfaces of the metal. AFM is required to obtain some quantitative data regarding the metal surface structure [49]. The roughness profile (ISO 4287), which lists specific criteria for the evaluation of surface roughness, is one of the texture forms currently established by the International Organization of Standardization (ISO) [50]. Fig. 10a, b indicates AFM images of corroded and inhibited Al alloy surface. Certain of them are R_a is the average surface roughness, as indicated by the arithmetic mean height, R_q is the root-mean-square roughness, and R_{max} is the average peak spacing profile irregularities. Table 6 provides the values of R_a, R_q and R_{max} for the examined the surfaces of Al alloy. Without inhibitors, the Al alloy sample was subjected to 0.1 M HCl solution, and as can be seen in Fig. 10a, this corrosive attack caused damage to the surface, which led to corrosion. The uncontrolled corroding surface had an average surface roughness of 226 nm. However, the average roughness was reduced by 35.4 nm and the surface became smoother when NTE was present, according to the AFM images in Fig. 10b. Increased surface smoothness in the presence of NTE suggests that the inhibitors have adhered to the surface of the aluminium alloy. The average roughness (Ra), root-mean-square (Rq) values, and observed surface roughness of the Al alloy dipped in 100 ppm NTE is much less than that dipped in 0.1 M HCl, shown in Table 6. It confirms the development of protective film of NTE on the Al surface.

3.6. Mechanism of inhibition

The inhibition activity of NTE in 0.1 M HCl solution against Al alloy, the corrosion depends on its adsorption on the alloy surface. As per the ΔG^o_{ads} values, NTE molecules basically undergoes mixed adsorption primarily with chemisorption. Generally, organic substances act as inhibitors to control the corrosion of metal or alloys through the adsorption process, which can take place on the surface
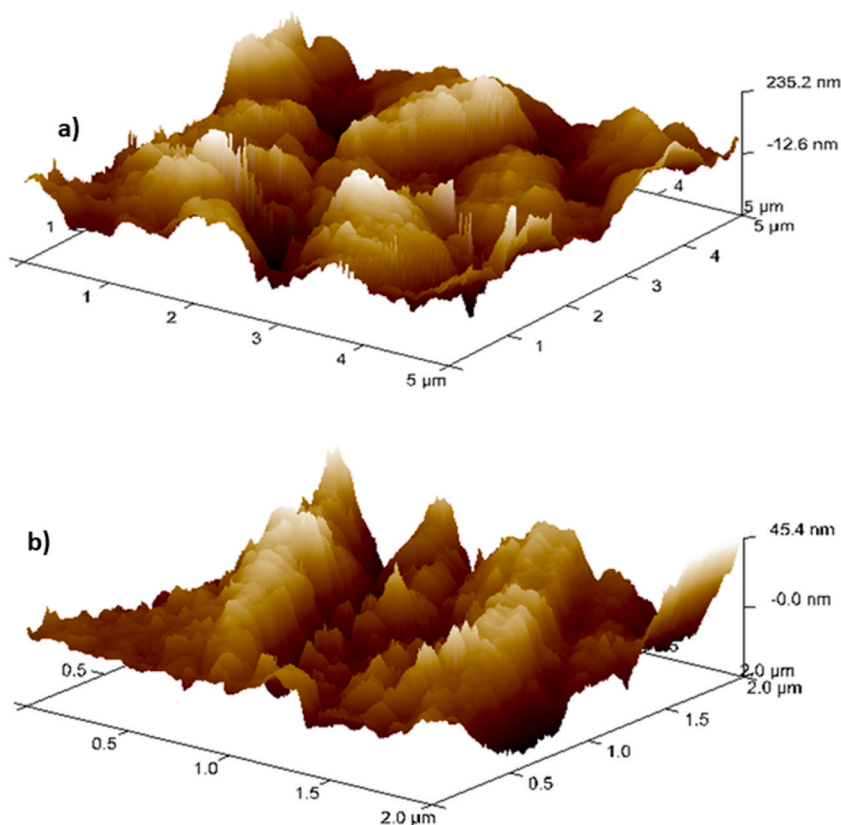
Fig. 10. 3D-AFM images of Al alloy dipped in a) 0.1 M HCl and b) dipped in 0.1 M HCl +100 ppm NTE.

Table 6
Results of the AFM study of Al in 0.1 M HCl without and with NTE.

Al alloy (AA6061)	R_a	R_q	R_{max}
Dipped in 0.1 M HCl	226 nm	294 nm	1815 nm
Dipped in 0.1 M HCl+ 100 ppm NTE	35.4 nm	18.2 nm	436 nm

of metals/alloy either through physisorption, chemisorption, or both type of adsorption of inhibitor on the surface of Al alloy. The extent of adsorption depends on the type of metal, and its surface quality, the chemical structure/composition of inhibitors, aggressiveness, and the temperature of the medium.
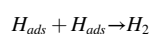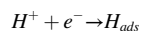
Physisorption is caused by the charged inhibitor species, and electrostatic attraction to the oppositely charged alloy surface (such as protonated species). While chemisorption can take place when an inhibitor and an empty d-orbital, metal atoms share a lone pair of electrons in heteroatoms or π-bonding electrons or an aromatic ring [51]. The O, N, and π -bonding electrons of heteroatoms of the aromatic ring in NTE certainly favor its chemisorption on the Al surface (Fig. 11.). The stronger adsorption can be achieved by using the N atoms of triazole, NO_2 functional group, and conjugated π-electrons of the aromatic ring as active adsorption centers. The NTE molecule might be responsible for the high degree of inhibition because it effectively adsorbs on a larger surface area of the alloy.

The following reactions can be used to reveal the electrochemical corrosion of Al in contact with the hydrochloric acid solution [52, 53].

Anodic reaction:

$$Al + Cl^- \leftrightarrows AlCl^-_{ads}$$

$$AlCl^-_{ads} + Cl^- \rightarrow AlCl^+_2 + 3e^-$$
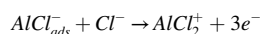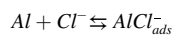
Cathodic reaction:

$$H^+ + e^- \rightarrow H_{ads}$$

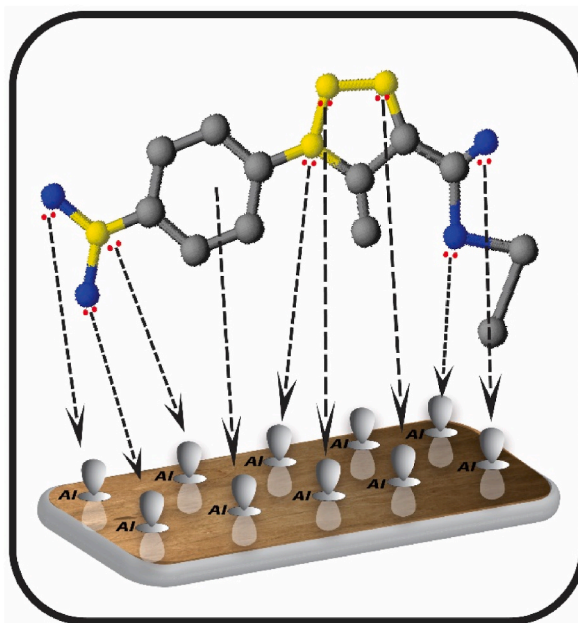$$H_{ads} + H_{ads} \rightarrow H_2$$

Fig. 11. Scheme of mechanism of NTE adsorption on Al alloy.

Generally, the improvement of an electric field at the metal/medium interface causes the metal surface in contact with an electrolyte solution to acquire an electric charge. Al has a pH_{Zch} value of 9.1 at no charge potential. Thus, in a very acidic media, Al alloy gains a positive charge, and negatively charged acidic Cl-ions are attracted to the positively charged alloy surface by electrostatic force [54,55]. NTE can be protonated in an acidic solution. The protonated NTE can easily attracted to the negatively charged Al alloy surface. Electrostatic adsorption of NTE on the alloy surface leads to physisorption. The chemisorption of NTE can be due to the sharing of lone pair electrons on O, N atoms and π-electrons of aromatic ring with the empty d-orbitals of Al alloy surface. From the potentiodynamic polarization data (Table 2), it indicates that the Tafel slopes increases with concentration of inhibitor, and hence I.E, increases during the corrosion process. From the EIS data (Table 3), indicates that the double layer capacitance value decreases with increase in inhibition efficiency.

3.7. Conclusion

Based on the investigation results, the following conclusions are made:

- NTE shows good inhibition efficiency on the AA6061 surface by forming a protective layer in 0.1 M HCl.
- The highest inhibition efficiency of 100 ppm solution was 94.2% at 333K, and it increased as NTE content and temperature increased.
- The potentiodynamic polarization and EIS methods produced results that were very similar. It is a mixed type of inhibitor.
- NTE followed Langmuir adsorption isotherm and got adsorbed on the surface of AA6061 through chemisorption. SEM and AFM analysis validated the formation of a protective layer.

Author contribution statement

Raviprabha K: Performed the experiments; wrote a paper.
Ramesh S. Bhat: Contributed reagents, materials, analysis tools or data.
Subrahamanya I. Bhat: Conceived and designed the experiments; Wrote a paper.
Nagaraja P: Analyzed and interpreted the data; Wrote the paper.
Jyothi K: Contributed reagents, materials, analysis tools or data; Wrote a paper.

Data availability statement

Data will be made available on request.

Ethics approval and consent to participate

Not applicable.

Consent for publication

Not applicable.

Declaration of competing interest

The authors declare the following financial interests/personal relationships which may be considered as potential competing interests:

Acknowledgements

Not applicable.

References

[1] W.S. Miller, L. Zhuang, J. Bottema, A.J. Wittebrood, P. De Smet, A. Haszier, A. Vieregge, Recent development in aluminium alloys for the automotive industry, Mater. Sci. Eng. A 280 (2000) 37–49.
[2] J. Fan, J Njuguna, An introduction to lightweight composite materials and their use in transport structures, in: J. Njuguna (Ed.), Lightweight Composite Structures in Transport, Design, Manufacturing, Analysis, and Performance, Woodhead Publishing, Elsevier Ltd, 2016, pp. 3–34.
[3] B. Xu, Y. Ji, X. Zhang, X. Jin, W. Yang, Y. Chen, Experimental and theoretical studies on the corrosion inhibition performance of 4-amino-N, N-di-(2-pyridylmethyl)-aniline on mild steel in hydrochloric acid, RSC Adv. 5 (2015) 56049–56059.
[4] R. Solmaz, Investigation of the inhibition effect of 5-((E)-4-phenylbuta-1,3-dienylideneamino) -1,3,4-thiadiazole-2-thiol Schiff base on mild steel corrosion in hydrochloric acid, Corrosion Sci. 52 (2010) 3321–3330.
[5] T. Zhang, S. Cao, H. Quan, Z. Huang, S. Xu, Synthesis, and corrosion inhibition performance of alkyl triazole derivatives, Res. Chem. Intermed. 41 (2013) 2709–2724.
[6] Q. Ma, S. Qi, X. He, Y. Tang, G. Lu, 1,2,3-Triazole derivatives as corrosion inhibitors for mild steel in acidic medium: experimental and computational chemistry studies, Corrosion Sci. 129 (2017) 91–101.
[7] M. Faisal, A. Saeed, D. Shahzad, N. Abbas, F. Ali Larik, P. Ali Channar, S. Aaliya Shehzadi, General properties, and comparison of the corrosion inhibition efficiencies of the triazole derivatives for mild steel, Corrosion Rev. 36 (2018) 507–545.
[8] J.R. Davis, Corrosion of Aluminium and Aluminium Alloys, ASM International, Ohio, 1999, https://doi.org/10.31399/asm.tb.caaa.9781627082990.
[9] U. Ergun, D. Yüzer, K.C. Emregül, The inhibitory effect of bis-2,6-(3,5,dimethylpyrazolyl) pyridine on the corrosion behaviour of mild steel in HCl solution, Mater. Chem. Phys. 109 (23) (2008) 492–499.
[10] P.B. Raja, M. Ismail, S. Ghoreishiamiri, J. Mirza, M.C. Ismail, S. Kakooei, A.A. Rahim, Reviews on corrosion inhibitors– a short view, Chem. Eng. Commun. 203 (2016) 1145–1156.
[11] J. Sharma, S. Ahmad, M.S. Alam, Bioactive triazoles: a potential review, J. Chem. Pharmaceut. Res. 4 (2012) 5157–5164.
[12] N. Phadke Swathi, V.D.P. Alva, S. Samshuddin, A review on 1,2,4-triazole derivatives as corrosion inhibitors, J. Bio- Tribo-Corrosion 3 (4) (2017) 42.
[13] Q. Ma, S. Qi, X. He, Y. Tang, G. Lu, 1,2,3-Triazole derivatives as corrosion inhibitors for mild steel in acidic medium: experimental and computational chemistry studies, Corrosion Sci. 129 (2017) 91–101.
[14] A. Zarrouk, B. Hammouti, S.S. Al-Deyab, R. Salghi, H. Zarrok, C. Jama, F. Bentiss, Corrosion inhibition performance of 3,5- diamino-1,2,4-triazole for protection of copper in nitric acid solution, Int. J. Electrochem. Sci. 7 (2012) 5997–6011.
[15] B.V.A. Rao, M.N. Reddy, B. Sreedhar, Self-assembled 1-octadecyl-1H-1,2,4-triazole films on copper for corrosion protection, Prog. Org. Coating 77 (2014) 202–212.
[16] F. El-Hajjaji, M. Messali, M.V. Martínez de Yuso, E. Rodríguez-Castellón, S. Almutairi, T.J. Bandosz, M. Algarra, Effect of 1-(3-phenoxypropyl) pyridazin-1-ium bromide on steel corrosion inhibition in acidic medium, J. Colloid Interface Sci. 541 (2019) 418–424.
[17] A. Boutouil, My R. Laamari, I. Elazhary, L. Bahsis, H. Anane, S.E. Stiriba, Towards a deeper understanding of the inhibition mechanism of a new 1,2,3-triazole derivative for mild steel corrosion in the hydrochloric acid solution using coupled experimental and theoretical methods, Mater. Chem. Phys. 241 (2020), 122420.
[18] M. Naciria, Y. El Aoufir, H. Lgaz, F. Lazrak, A. Ghanimi, A. Guenbour, I.H. Alie, M. El Moudanea, T. Jamal, Ill-Min Chung, Exploring the potential of a new 1,2,4-triazole derivative for corrosion protection of carbon steel in HCl: a computational and experimental evaluation, Colloids Surf., A 597 (2020), 124604.
[19] M. Murmu, S. Kr Saha, P. Bhaumick, N.C. Murmu, H. Hirani, P. Banerjee, Corrosion inhibition property of azomethine functionalized triazole, derivatives in 1 mol L−1 HCl medium for mild steel: experimental and theoretical exploration, J. Mol. Liq. 313 (2020), 113508.
[20] K. Xhanari, M. Finsgar, Organic corrosion inhibitors for aluminium and its alloys in acid solutions: a review, RSC Adv. 6 (2016) 62833–62857.
[21] K. Xhanari, M. Finsgar, The corrosion inhibition of AA6082 aluminium alloy by certain azoles in chloride solution: electro- chemistry and surface analysis, Coatings 9 (2019) 380.
[22] P. Shetty, Schiff bases: an overview of their corrosion inhibition activity in acid media against mild steel, Chem. Eng. Commun. 207 (2020) 985–1029.
[23] Q. Zhao, T. Tang, P. Dang, Z. Zhang, F. Wang, The corrosion inhibition effect of triazinedithiol inhibitors for aluminium alloy in a 1M HCl solution, Metals 7 (2017) 1–11.
[24] S. Bala, N. Sharma, A. Kajal, S. Kamboj, V. Saini, Mannich Bases: an important pharmacophore in present scenario, Inter. J. Med. Chem. (2014) 1–14.
[25] K. Raviprabha, R.S. Bhat, Inhibition effects of ethyl-2-amino-4-methyl-1,3-thiazole-5 carboxylate on the corrosion of AA6061 alloy in hydrochloric acid media, J. Fail. Anal. Prev. 19 (2019) 1464–1474.
[26] P.P. Kumari, P.N. Shetty, D. Sunil, Effect of cysteine as environmentally friendly inhibitor on AA6061-T6 corrosion in 0.5 M HCl Electrochemical and Surface Studies, Surf. Eng. Appl. Electrochem. 56 (2020) 624–634.
[27] K. Raviprabha, R.S. Bhat, Electrochemical and quantum chemical studies of 5- [(4 Chlorophenoxy) Methyl]-4H-1,2,4-Triazole-3-Thiol on the corrosion inhibition of 6061 Al alloy in hydrochloric acid, J. Fail. Anal. Prev. 20 (5) (2020) 1598–1608.
[28] B.P. Charitha, P. Rao, Electrochemical and adsorption studies for the corrosion control of 6061 Al alloy using eco-friendly inhibitor, Surf. Eng. Appl. Electrochem. 53 (2017) 551–559.
[29] G.M. Pinto, J. Nayak, A. Nityananda Shetty, Corrosion inhibition of 6061 Al–15 vol. pct. SiC(p) composite and its base alloy in a mixture of sulphuric acid and hydrochloric acid by 4-(N, N dimethyl amino) benzaldehyde thiosemicarbazone, Mater. Chem. Phys. 125 (2010) 628–640.
[30] P.N. Shetty, P.P. Kumari, Inhibitive action of glutathione reduced on the deterioration of AA6061 in 0.5M HCl, Tribol. Ind. 42 (2020) 214–224.
[31] M. Abdallah, Antibacterial drugs as corrosion inhibitors for corrosion of aluminium in hydrochloric solution, Corrosion Sci. 46 (2004) 1981–1996.

[32] E.A. Noor, Evaluation of inhibitive action of some quaternary N-heterocyclic compounds on the corrosion of Al–Cu alloy in hydro chloric acid, Mater. Chem. Phys. 144 (2009) 533–541.

[33] A. Yurt, S. Ulutas, H. Dal, Electrochemical and theoretical investigation on the corrosion of aluminium in acidic solution containing some Schiff bases, Appl. Surf. Sci., 253 (2006) 919–925.

[34] W.H. Li, Q. He, S.T. Zhang, C.L. Pei, B.R. Hou, Some new triazole derivatives as inhibitors for mild steel corrosion in acidic medium, J. Appl. Electrochem. 38 (2008) 289–295.

[35] H. Fathima, M. Pais, P. Rao, Anticorrosion performance of biopolymer pectin on 6061 aluminium alloy: electrochemical, spectral and theoretical approach, J. Mol. Struct. 1243 (2021), 130775.

[36] Y. Qiang, S. Zhang, H. Zhao, B. Tan, L. Wang, Enhanced anticorrosion performance of copper by novel N-doped carbon dots, Corrosion Sci. 161 (2019), 108193.

[37] M. Metikos-Hukovic, R. Babic, Z. Grubac, Corrosion protection of aluminium in acidic chloride solutions with nontoxic inhibitors, J. Appl. Electrochem. 28 (1998) 433–439.

[38] C.M.A. Brett, The application of electrochemical impedance techniques to aluminium corrosion in acidic chloride solution, J. Appl. Electrochem. 20 (1990) 1000–1003.

[39] C.M.A. Brett, On the electrochemical behaviour of aluminium in acidic chloride solution, Corrosion Sci. 33 (1992) 203–210.

[40] K. Raviprabha, R.S. Bhat, 5-(3-Pryridyl)-4H-1,2,4-triazole-3-thiol as potential corrosion inhibitor for AA6061 aluminium alloy in 0.1M hydrochloric acid solution, Surf. Eng. Appl. Electrochem. 55 (6) (2019) 723–733.

[41] F.O. Nwosu, M.M. Muzakir, Thermodynamic and adsorption studies of corrosion inhibition of mild steel using lignin from siam weed (*Chromolaena odorata*) in acid medium, J. Mater. Environ. Sci. 7 (2016) 1663–1673.

[42] N. Hebbar, B.M. Praveen, B.M. Prasanna, T. Venkatesha, Corrosion inhibition behaviour of ketosulfone for zinc in acidic medium, J. Fund. Appl. Sci. 7 (2015) 271–289.

[43] E.E. Oguzie, Corrosion inhibition of aluminium in acidic and alkaline media by Sansevieria trifasciata extract, Corrosion Sci. 49 (2007) 1527–1539.

[44] N. Arrousse, E. Mabrouk, R. Salim, K. Ismaily Alaoui, F. El Hajjaji, Z. Rais, M. Taleb, B. Hammouti, Fluorescein as commercial and environmentally friendly inhibitor against corrosion of mild steel in molar hydrochloric acid medium, Mater. Today Proc. 27 (2020) 3184–3192.

[45] I.B. Obot, E.E. Ebenso, M.M. Kabanda, Metronidazole as environmentally safe corrosion inhibitor for mild steel in 0.5M HCl: experimental and theoretical investigation, J. Environ. Chem. Eng. 1 (2013) 431–439.

[46] M.A. Amin, M.A. Ahmed, H.A. Arida, T. Arslan, M. Saracoglu, F. Kandemirli, Monitoring corrosion and corrosion control of iron in HCl by non-ionic surfactants of the TRITON-X series-Part II. Temperature effect, activation energies and thermodynamics of adsorption, Corrosion Sci. 53 (2011) 540–548.

[47] M.A. Quraishi, J. Rawat, M. Ajmal, Dithiobiurets: a novel class of acid corrosion inhibitors for mild steel, J. Appl. Electrochem. 30 (2000) 745–751.

[48] Z. Salarv, M. Amirnasr, M. Talebian, K. Raeissi, S. Meghdadi, Enhanced corrosion resistance of mild steel in 1M HCl solution by trace number of 2-phenyl-benzothiazole derivatives: experimental, quantum chemical calculations and molecular dynamics (MD) simulation studies, Corrosion Sci. 114 (2017) 133–145.

[49] F. Bentiss, M. Lebrini, M. Lagrenee, Thermodynamic characterization of metal dissolution and inhibitor adsorption processes in mild steel/2,5-bis (n-thienyl)-1,3,4-thiadiazoles/hydrochloric acid system, Corrosion Sci. 47 (2005) 2915–2931.

[50] G. Bereket, A. Pinarbsi, Electrochemical thermodynamic and kinetic studies of the behaviour of aluminium in hydrochloric acid containing various benzotriazole derivatives, Corrosion Eng. Sci. Technol. 39 (2004) 308–312.

[51] S. Sharma, A. Kumar, Recent advances in metallic corrosion inhibition: a review, J. Mol. Liq. 322 (2021), 114862.

[52] S.A. Umoren, M.M. Solomon, Madhankumar, et al., Exploration of natural polymers for use as green corrosion inhibitors for AZ31 magnesium alloy in saline environment, Carbohydr. Polym. 230 (2020), 115466.

[53] G. Bereket, A. Pinarbasi, Electrochemical thermodynamic and kinetic studies of the behaviour of aluminium in hydrochloric acid containing various benzotriazole derivatives, Corrosion Eng. Sci. Technol. 39 (4) (2004) 308–312.

[54] P.P. Kumari, P.N. Shetty, D. Sunil, Effect of cysteine as environmentally friendly inhibitor on AA6061-T6 corrosion in 0.5 M HCl: electro- chemical and Surface Studies, Surf. Eng. Appl. Electrochem. 56 (5) (2020) 624–634.

[55] A.A. El-Awady, B.A. Abd-El-Nabey, S.G. Aziz, Thermodynamic and kinetic factors in chloride ion pitting and nitrogen donor ligand inhibition of aluminium metal corrosion in aggressive acid media, J. Chem. Soc., Faraday Trans. 89 (5) (1993) 795–802.